The collapse of genetic incompatibilities in a hybridizing population

Tianzhu Xiong*[1] and James Mallet[1]

[1] *Department of Organismic and Evolutionary Biology, Harvard University, Cambridge, MA 02138*

January 8, 2021

Abstract

Genetic incompatibility has long been considered to be a hallmark of speciation due to its role in reproductive isolation. Previous analyses of the stability of epistatic incompatibility show that it is subject to collapse upon hybridization. In the present work, we derive explicitly the distribution of the lifespan of two-locus incompatibilities, and show that genetic drift, along with recombination, is critical in determining the time scale of collapse. The first class of incompatibilities, where derived alleles separated in parental populations act antagonistically in hybrids, survive longer in smaller populations when incompatible alleles are (co)dominant and tightly linked, but collapse more quickly when they are recessive. The second class of incompatibilities, where fitness is reduced by disrupting co-evolved elements in gene regulation systems, collapse on a time scale proportional to the exponential of effective recombination rate. Overall, our result suggests that the effects of genetic drift and recombination on incompatibility's lifespan depend strongly on the underlying mechanisms of incompatibilities. As the time scale of collapse is usually shorter than the time scale of establishing a new incompatibility, the observed level of genetic incompatibilities in a particular hybridizing population may be shaped more by the collapse than by their initial accumulation. Therefore, a joint theory of accumulation-erosion of incompatibilities is in need to fully understand the genetic process under speciation with hybridization.

A. INTRODUCTION

Hybrid incompatibility, where two or more genetic elements interfere with each other to reduce the fitness of some hybrid genotypes, is a common phenomenon seen between diverging populations [1]. Early theories proposed simple models to explain a wide class of incompatibilities. The classical model studied involves two loci, each with derived alleles separated in different species that interact antagonistically upon hybridization, known as Dobzhansky-Muller incompatibilities (DMIs. In the following text we use "DMI" interchangeably with "hybrid incompatibility") [2, 3, 4, 5]. Genetic incompatibilities have been assumed to be important sources of reproductive isolation and the maintenance of species boundaries, as they provide a plausible mechanism to reduce the amount of gene flow between incipient species that can still hybridize [6], as well as the selection pressure for reinforcement (the evolution of assortative mating to avoid production of unfit hybrids) [7].

Intuitively, it may seem that any hybrid incompatibility will resemble the effect of an underdominant locus by reducing the fitness of hybrids, and will maintain reproductive isolation. However, incompatibilities in many classical DMI models are in fact unstable, and will begin to decay immediately after the onset of hybridization [8]. The reason for the collapse of classical DMIs is simply that the ancestral haplotype can be recreated by recombination in the hybrids. This haplotype achieves the highest marginal fitness because of its compatibility with all other haplotypes. Selection in favor of the ancestral haplotype decreases the frequency of derived alleles, and hence drives the collapse

of incompatibility. This observation has inspired several results on the conditions for the long term stability of classical DMIs: in most cases the derived allele needs to be sufficiently divergently selected to resist purging [9, 10].

Until now, the stochastic processes of the collapse of DMIs upon hybridization have remained largely neglected. As many classical DMIs are unstable in the long term, they may not provide an effective mechanism to maintain reproductive isolation between species. However, recent empirical studies have suggested that the pattern of DMIs in hybridizing populations can be very complex. Hybrid incompatibility may correlate more with geographic distribution than with species relationship. For instance, two parapatric populations of the butterfly *Heliconius pardalinus* are found to produce sterile F_1 females in both directions of cross, and yet hybrids between *H. pardalinus* and the sympatric *H. elevatus* are completely fertile, likely because interspecific gene flow has purged the incompatibility in sympatry [11]. In another case, the temporal dynamics of DMI in hybrids shows cryptic metastability: a two-locus classical DMI between two hybridizing monkeyflowers *Mimulus guttatus* and *M. nasutus* appears to have persisted for much longer than expected under deterministic theory [12]. If hybridization began only recently, it may not have had sufficient time to purge classical DMIs from the population [13]. There are also other forms of DMI, most notably those evolved under developmental system drift [14, 15], that can be more stable than the classical ones [16, 17]. Correctly interpreting data from systems like these requires a more precise understanding of the stochastic dynamics of DMIs in hybridizing populations. In particular, the joint influence of noise (genetic drift), selection and recombination on the temporal dynamics of DMIs subject to hybridization has remained elusive in analytical theory.

To address these problems, our main question becomes: what is the time course of the collapse of a DMI during hybridization? Specifically, we will quantify how the time course of DMI collapse depends on: 1) the strength of genetic drift and recombination; 2) the underlying mechanism of incompatibility. We will also investigate the possibility of recovering a DMI if hybridization ends. We build a stochastic model based on an ecologically motivated birth-death process in a focal population that hybridizes with a source (Figure 1). We consider only two-locus incompatibilities as they are often the first kind of DMI to appear between incipient species [5], and they are also the easiest to identify empirically. We will present the analytical approximation to the distribution of the collapse time, or the mean collapse time, under different schemes of DMI, and show how genetic drift and recombination alter the time scale of a DMI's lifespan. We show that metastability is a likely outcome with DMIs evolved under compensated developmental system drift between regulatory elements, where higher recombination rates facilitates the segregation and the survival of incompatibilities.

B. MODELS AND RESULTS

The diploid birth-death process

To approximate the stochastic detail of population biology, our model is built on the population dynamics of a continuous-time birth-death process with monoecious, diploid individuals containing two bi-allelic loci (a/A, b/B) that recombine with probability r (see Materials and Methods). We set up a population structure resembling the source-sink model [18] where the influence of gene flow is unidirectional from the source into the focal (sink) population as a result of hybridization (Figure 1). The source population is assumed to remain at constant allele frequencies and at linkage equilibrium, a reasonable approximation for evolution in a large panmictic species, which interacts with a peripheral focal population. The focal population is initially fixed for the focal haplotype. With on-going hybridization, the depletion of its focal haplotype indicates the collapse of DMI.

Importantly, we consider hybridization as rare (e.g. the probability of cross-population mating $m \lesssim 0.05$) but recurrent. This is a reasonable assumption for populations with strong mate-preference towards their own types, or are divided by strong spatial barriers. With this assumption, the frequencies of incompatible genotypes in the focal population will be low so that their impact on the population size can be neglected. We then transform the stochastic process from genotype

Table 1: Glossary of symbols

Original model: the birth-death process	
Parameter	**Meaning**
α	Reproduction rate
μ	Baseline mortality rate
β	Density dependent mortality rate
s_j	Mortality rate due to viability selection on genotype j
m	Hybridization probability
r	Recombination probability
Variable	**Meaning**
n_j	The number of individuals of genotype j
t	Time
Approximation: stochastic differential equations	
Parameter	**Meaning**
N	Equilibrium population size under neutrality, $(\alpha - \mu)/\beta$
λ	Gene flow rate, $\alpha m/2$
ω	Recombination rate, $\alpha r(1 - m/2)$
γ	Relative recombination rate, ω/λ
θ_k^*	Frequency of haplotype k in the source population (fixed)
Variable	**Meaning**
θ_k	Frequency of haplotype k in the focal population
ξ_{θ_k}	Noise on θ_k (genetic drift)
τ	Time scaled by the rate of gene flow, λt
T_d	Collapse time of DMI

numbers to haplotype frequencies θ_k and the total population size N as deviation from Hardy-Weinberg equilibrium has minimal impact on the dynamics (SI Appendix A). This approach reduces the number of state variables and allows us to define the rate of gene flow as λ, and the rate of recombination as ω. Time t is scaled by the gene flow rate such that $\tau = \lambda t$ captures the relative time scale of collapse. The relative recombination rate is defined as $\gamma = \omega/\lambda$. From now on, all of our results are discussed with respect to the relative time τ. With these assumptions, a system of stochastic differential equations on θ_k, equipped with inter-correlated noises $\xi_{\theta_k}(\tau)$, can be formulated to fully describe the evolution of state variables $\boldsymbol{\theta} = (\theta_0, \theta_1, \theta_2, \theta_3)$, corresponding to the frequencies of haplotype AB, Ab, aB and ab in the focal population. The equation details are given in Materials and Methods, and SI Appendix A.

Ultimately, we are interested in the statistical properties of the collapse time T_d at which the focal haplotype is purged from the focal population:

$$T_d = \inf\{\tau \geq 0 | \theta_{\text{focal haplotype}}(\tau) = 0\} \tag{1}$$

Models of incompatibilities

In what we here call "classical DMIs", it is assumed that the ancestral genotype of both populations is $ab|ab$. In one such population, a derived allele A may be substituted at one of the loci, and allele B at the other. Often, this is conceived of occurring even in the absence of selection against (or for) either substitution, giving a "holey landscape" fitness model [19]. However in hybrids, alleles A and B interact antagonistically to give low fitness defined via dominance coefficients of derived alleles.

Another major type of DMI arises from explicitly considering molecular interactions [20, 21, 16]. For instance, a *cis*-regulatory element affects only its target gene(s) on the same chromosome, but has no control over the same gene on the homologous chromosome.

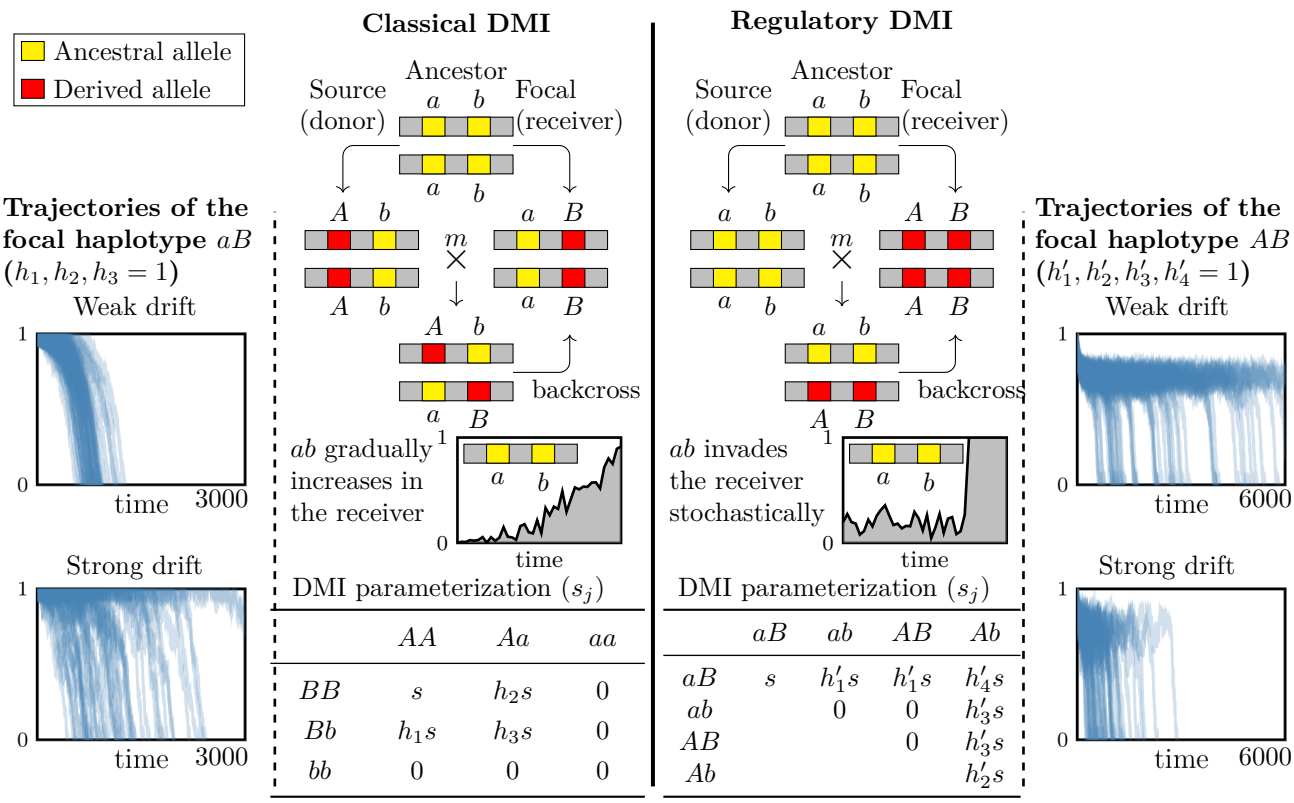

	AA	Aa	aa
BB	s	$h_2 s$	0
Bb	$h_1 s$	$h_3 s$	0
bb	0	0	0

	aB	ab	AB	Ab
aB	s	$h'_1 s$	$h'_1 s$	$h'_4 s$
ab		0	0	$h'_3 s$
AB			0	$h'_3 s$
Ab				$h'_2 s$

Figure 1: Models of two-locus DMIs. Red (derived) and yellow (ancestral) blocks represent different alleles. The classical DMI consists of one derived allele at each locus in each separate population. The ancestral haplotype ab can be recovered by recombination (with probability r) upon hybridization (with probability m). The collapse is mainly characterized by a gradual increase of the ancestral haplotype ab in the focal population. The regulatory DMI consists of two derived alleles in the same population (possibly evolved via gradual co-evolutionary drift of the regulatory element with the genes they control). The invading haplotype ab stochastically crosses an unstable threshold frequency in the focal population by escaping recombination that breaks apart the co-adapted haplotype; it then sweeps to fixation. The strength of incompatibilities (s_j) is parameterized in the table below each type. The regulatory DMI requires a haplotype-explicit selection regime, while the classical DMI relies only on dominance at each locus. Although there are a large number of coefficients for each regime, the dynamics of collapse depends only weakly on the details of incompatibilities if selection is sufficiently strong ($s/\alpha \gg 1$). Ensembles of the trajectories of the focal haplotype are presented on the left side for classical DMIs, and on the right side for regulatory DMIs ($\alpha = 1$, $\mu = 0.1$, $\beta = 9 \times 10^{-5}$ or 9×10^{-4} such that the equilibrium population size is $N = 10^4$ for weak drift, and $N = 10^3$ for strong drift; $m = 0.01$, $s = 10$, and $h_1, \cdots, h_3, h'_1, \cdots, h'_4$ are all 1. $r = 0.25$ for classical DMI and $r = 0.055$ for regulatory DMI).

Interactions of this kind have previously been shown in simulations to be effective at maintaining gene flow barriers [17]. Co-adapted pairs of *cis*-regulatory elements and their target genes represent some of the simplest examples of metastable systems in evolution, where selection favors the coupling of a few particular combinations of alleles, leading to high levels of linkage disequilibrium [22]. Experiments have also shown that divergence via *cis*-regulatory change is frequently observed between sister species, which is sometimes compensated for by associated *trans*-regulatory change [23, 24]. Incompatibilities via regulatory co-evolution is not well modeled using classical DMIs, and will be hitherto referred to as "regulatory DMIs", where derived alleles A and B co-occur in the same population.

We formulate the incompatibilities in our model by specifying s_j, the genotype-specific mortality rate, and confine the analysis to autosomal interactions. For clas-

sical DMIs, s_j is described by a four-parameter fitness landscape where s is the strength of incompatibility, and h_1, h_2, h_3 represent dominance (Figure 1, left). For incompatibilities involving *cis*-regulatory elements, we must distinguish $s_{Aa|Bb}$ from $s_{AB|ab}$ and the fitness is calculated based on whether each haplotype has a matching regulatory element and gene target, where $h'_1, \cdots, h'_4$ determine the selection on various genotypes containing mismatched haplotypes (Figure 1, right).

Dynamics under strong incompatibilities

To analytically quantify the time scale of collapse, we here present the haplotype dynamics under strong incompatibilities ($s \gg \alpha$). As selection against incompatibilities acts on a faster time scale than hybridization, incompatible genotypes cannot rise to considerable frequencies in the population. Therefore, at any moment, the focal population consists mostly of inter-compatible haplotypes and is largely neutral. These assumptions enable us to focus on the dynamics of just one haplotype per two-locus system. Furthermore, the impact of incompatibilities on the population size is small because hybrids are rare, such that it remains approximately at its equilibrium value $N = (\alpha - \mu)/\beta$. For the same reason, the noise satisfies $\langle \xi_{\theta_k}(\tau)\xi_{\theta'_k}(\tau')\rangle = \alpha N^{-1}\theta_k(\delta_{k,k'} - \theta'_k)\delta(\tau - \tau')$.

Classical DMIs. For classical DMIs, the focal population consists mostly of haplotypes aB (focal) and ab (ancestral) in the course of collapse. We show in SI Appendix B that if A is (co)dominant, the frequency of haplotype aB is approximated by the following stochastic differential equation:

$$\partial_\tau \theta_2 = \theta_1^* \left[2\theta_2 - 1 - \frac{\frac{\omega}{s}\theta_2}{(\frac{\omega}{s} + h_3)\theta_2 + \frac{h_3}{h_2}(\frac{2\omega}{s} + h_3)(1 - \theta_2)} \right] - \theta_2 + \xi_{\theta_2}(\tau)/\sqrt{\lambda}, \tag{2}$$

from which we can directly calculate the initial rate of collapse: $\partial_\tau \langle \theta_2 \rangle|_{\theta_2=1} = -\frac{\omega/s + (1-\theta_1^*)h_3}{\omega/s + h_3}$. This has several immediate implications. If incompatibility is strong so that $\omega/s \ll h_3$, the initial rate of collapse depends strongly on $(1 - \theta_1^*)$, i.e., whether A is fixed in the source population or not. With a completely fixed A, the initial rate is on the order of ω/s, which corresponds to the rate of generating the first ancestral haplotype ab from an F_1 hybrid that has escaped incompatibility and subsequently produced a recombinant ab gamete. If A is not fixed in the source population, the first occurrence of the ancestral haplotype ab is almost independent of selection, and the rate of collapse will be largely determined by the frequency of the ancestral haplotype in the source population, which depends only on $(1 - \theta_1^*)$. Thus, selection against hybrids when allele A is (co)dominant does not strongly influence a classical DMI's initial collapse unless the ancestral haplotype is initially absent everywhere.

If A and B are both recessive, the dynamics of θ_2 are controlled mainly by the relative recombination rate γ:

$$\partial_\tau \theta_2 = \left(\frac{\theta_1^* \gamma}{1 + \gamma} - 1 \right) \theta_2 - \frac{\theta_1^* \gamma}{1 + \gamma} + \xi_{\theta_2}(\tau)/\sqrt{\lambda} \tag{3}$$

Regulatory DMIs. For regulatory DMIs, strong selection against incompatibility preserves mostly the two functional haplotypes ab and AB in the focal population. The asymptotic method in SI Appendix B leads to the following stochastic differential equation for the frequency θ_0 of haplotype AB:

$$\partial_\tau \theta_0 = -\theta_0 - \gamma\theta_0(\theta_0 - 1)(2\theta_0 - 1) + \xi_{\theta_0}(\tau)/\sqrt{\lambda} \tag{4}$$

This equation holds regardless of the details of incompatibilities in each genotype as long as it is present in all recombinant backcrosses ($h'_1, \cdots, h'_4 > 0$), and so it is valid not only for DMIs between *cis*-regulatory elements and their target genes, but also for DMIs between *trans*-regulatory elements and their targets, so long as the F_1 genotype $ab|AB$ is relatively fit, a reasonable assumption if gene regulation is largely linear [15]. Unlike classical DMIs, regulatory DMIs can be metastable depending on the relative recombination rate γ. For [4], the necessary and sufficient condition for the existence of a metastable frequency requires $\gamma > 8$, which translates to

$$m < 2r/(8 + r) \lesssim 0.12 \tag{5}$$

In other words, to achieve metastability in a two-locus regulatory DMI, the probability of hybridization has a

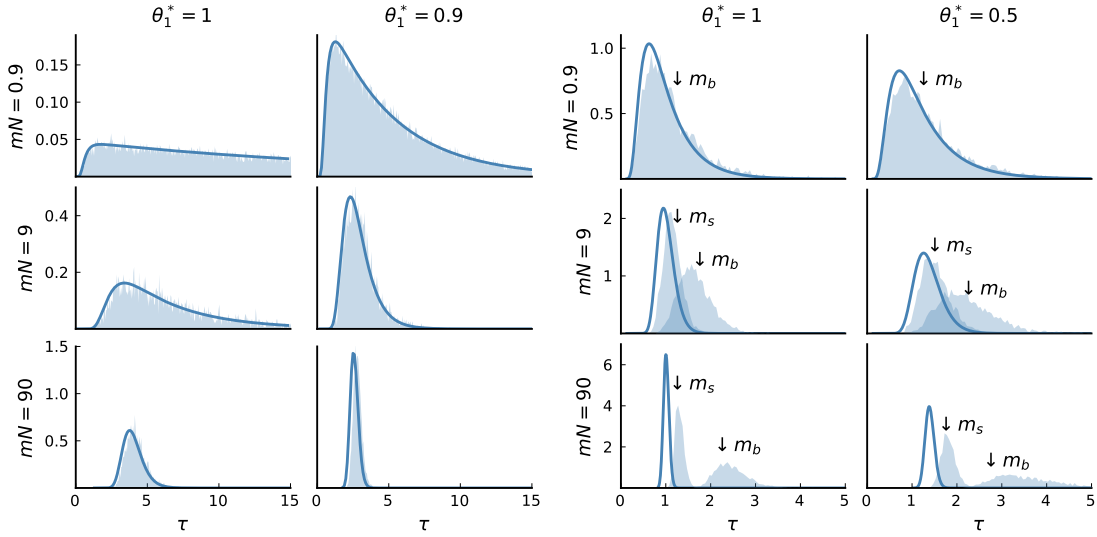

(a) $f_{T_d}(\tau)$, Dominant → Dominant

(b) $f_{T_d}(\tau)$, Recessive → Recessive

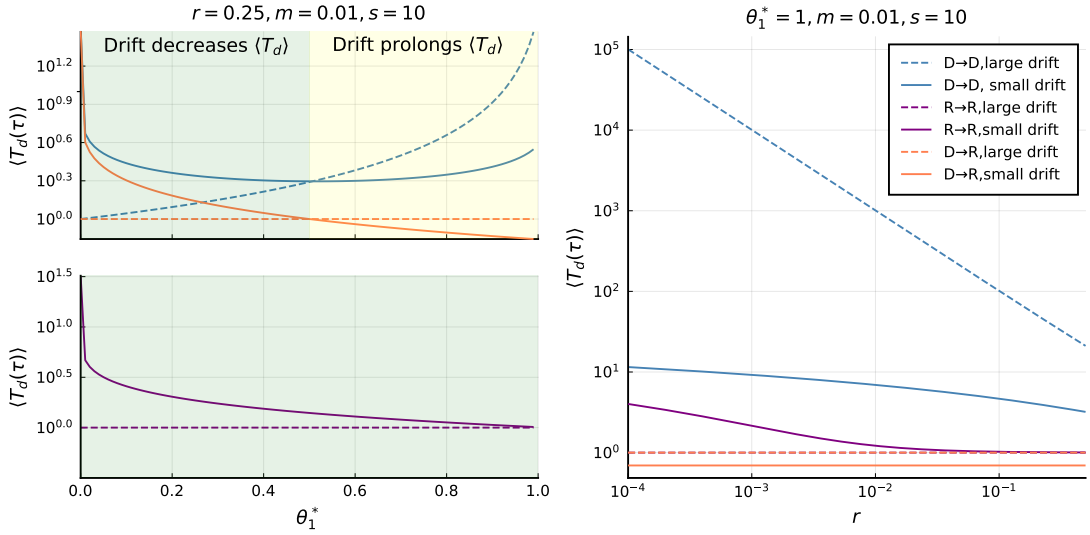

(c) $\langle T_d \rangle$ as a function of θ_1^* (left panel) and recombination probability r (right panel)

Figure 2: The distribution and the mean of the collapse time under classical DMIs. **(a, b)** The distribution of T_d from simulation and formula [6] under the classical DMI. The theoretical distribution $f_{T_d}(\tau)$ is shown in solid curves and the simulated distributions are shown in colored histograms. These parameters are held fixed: $\alpha = 1, \mu = 0.1, s = 10, r = 0.25$. A realistic hybridization probability $m_b = 10^{-2}$ is used in all simulations. In some cases we also added the results with a smaller probability $m_s = 10^{-5}$ (marked explicitly). As mN is an effective parameter in the expression of $f_{T_d}(\tau)$, for different m, we adjust the density-dependent mortality rate β to alter the equilibrium population size N, such that mN is held at three fixed values shown on the y-axis. Formula [6] approximates the simulations well when incompatibilities involve two dominant alleles, but it underestimates T_d in recessive-recessive DMIs. However, with stronger genetic drift or smaller hybridization probabilities, the empirical distribution converges to [6] even in the latter case. **(c)** The limiting values of $\langle T_d \rangle$ under strong/weak genetic drift (D=dominant, R=recessive). In general, populations with smaller genetic drift have longer $\langle T_d \rangle$ if the invading allele segregates at frequencies $\theta_1^* < 0.5$ in the source population. However, if the invading allele is (co)dominant and also has a source frequency $\theta_1^* > 0.5$, populations with stronger genetic drift have significantly longer $\langle T_d \rangle$. **(d)** Recombination decreases the average lifespan of classical DMIs, and the effect is most prominent for dominant-dominant interactions with strong genetic drift.

global upper-bound ≈ 0.12 that is independent of the details of incompatibility as long as it is strong and present in all recombinant backcrosses. For a particular system with recombination probability r between two DMI loci, the upper-bound is approximately $r/4$. However, especially in a small peripheral population, genetic drift can breach through the metastable frequency and lead to the collapse of regulatory DMIs.

Low recombination and strong genetic drift can prolong the lifespan of (co)dominant classical DMIs

The mean collapse time $\langle T_d \rangle$ quantifies the average lifespan of genetic incompatibilities under hybridization, and it is a good measure of the time scale of collapse. Here we first calculate the distributions of T_d under different classical DMIs, and then compare their average values.

Calculating the distribution of collapse time is a first-passage problem in diffusion theory [25, 26]. As [2] is approximately linear in θ_2 under strong incompatibilities, both [2] and [3] take the linear form $\partial_\tau \theta_2 = u_1\theta_2 - u_2 + \xi_{\theta_2}(\tau)/\sqrt{\lambda}$, where u_1, u_2 are constants defined by the parameters of the model, as shown in Table 2. Following the procedure in SI Appendix C, the general solution to the collapse time distribution is then

$$f_{T_d}(\tau) = \sum_{i=0}^{\infty} \frac{(-1)^i (2i + 2\tilde{u}_2 - \tilde{u}_1 + 1)\Gamma(i + 2\tilde{u}_2 - \tilde{u}_1 + 1)}{mNi! e^{\nu_i \tau}\Gamma(\tilde{u}_2 - \tilde{u}_1)\Gamma(\tilde{u}_2 + 1)} \tag{6}$$

where the compound parameters $\tilde{u}_1, \tilde{u}_2$, and the eigenvalues ν_i of the forward diffusion are given by

$$\begin{aligned} &\tilde{u}_1 = mNu_1; \quad \tilde{u}_2 = mNu_2 \\ &\nu_i = (mN)^{-1}(i + \tilde{u}_2 + 1)(i + \tilde{u}_2 - \tilde{u}_1) \end{aligned} \tag{7}$$

The physical meanings of u_1, u_2 are related to a DMI's collapse rate. $u_2 - u_1$ quantifies the initial rate of collapse, and u_2 itself measures the final rate of collapse. If $u_1 > 0$, the collapse is a self-accelerating process — initiating the collapse is slow, but once initiated it quickly sweeps through the population. The best example of self-accelerating collapse is when both derived alleles are dominant, because accumulating the ancestral haplotype ab in the focal population eases the formation of viable F_1 hybrids that then introduce more ancestral haplotypes. If $u_1 < 0$, the collapse is initially quick, but its rate gradually diminishes through time. In classical DMI models, decelerating collapse can be seen if the derived haplotype in the source population is segragating at a minor frequency ($\theta_1^* < 0.5$).

To validate the accuracy of the analytical approximation of $f_{T_d}(\tau)$, we simulated the exact birth-death process with dominant-dominant and recessive-recessive interactions. The results shown in Figure 2a, 2b confirm that the approximation is fairly accurate for small hybridization probabilities, and it holds for all levels of genetic drift. Particularly, at the strong drift limit, higher order eigenvalues rapidly dissipate from the distribution, and $f_{Td}(\tau)$ is essentially characterized by the slowest component, which is an exponential distribution: $\lim_{mN\to 0} f_{T_d}(\tau) \to (u_2 - u_1)e^{-(u_2-u_1)\tau}$

Our approximation for the classical DMI yields the following mean collapse time:

$$\langle T_d \rangle = mN[\psi(\tilde{u}_2 + 1) - \psi(\tilde{u}_2 - \tilde{u}_1)]/(1 + \tilde{u}_1), \tag{8}$$

where ψ is the digamma function (SI Appendix C). The values of $\langle T_d \rangle$ under different schemes of dominance and recombination probabilities are summarized in Figure 2c and Table S2 in SI Appendix C.

As recombination facilitates creating the ancestral haplotype, it will always reduce the mean collapse time of classical DMIs (Figure 2c, right). At the limit of strong genetic drift, the mean collapse time only depends on the initial collapse rate due to its exponential feature: $\langle T_d \rangle \approx (u_2 - u_1)^{-1}$. When genetic drift is weak, the mean collapse time depends on both the initial and the final rate of collapse: $\langle T_d \rangle \approx \frac{1}{u_1} \ln \frac{u_2}{u_2 - u_1}$.

That the time scale depends more heavily on the initial dynamics of the system in small populations is consistent with the result from diffusion theory, where allele frequency distributions are U-shaped when genetic drift dominates other forces [18]. Collapse under strong genetic drift can be viewed as the stochastic escape from the initial state $\theta_2 = 1$. An interesting corollary is that genetic drift on average prolongs the lifespan of a DMI when its collapse is self-accelerating, but decreases the

Table 2: Values of u_1, u_2 under different schemes of classical DMI

Dominance	u_1	u_2
(Co)dominant A & (co)dominant B	$-\frac{\omega/s+(1-\theta_1^*)h_3}{\omega/s+h_3}+\theta_1^*$	θ_1^*
(Co)dominant A & recessive B	$2\theta_1^*-1$	$2\theta_1^*$
Recessive A & recessive B	$\frac{\theta_1^*\gamma}{1+\gamma}-1$	$\frac{\theta_1^*\gamma}{1+\gamma}$

lifespan when collapse is decelerating (Figure S2 in SI Appendix). For instance, the self-accelerating collapse of dominant-dominant DMIs with $\theta_1^*=1$ has an average lifespan of s/ω under strong genetic drift, while it is reduced to $\ln(s/\omega)$ if genetic drift is weak. If s/ω is very large, the difference between the two scenarios will be significant. Consequently, rare hybridization will have a very small impact on the survival of dominant-dominant DMIs when both DMI alleles are initially fixed in each population. It predicts a much longer persistence than that under deterministic theories [8, 9].

High recombination and weak genetic drift can lead to persistent metastable regulatory DMIs

In classical DMIs, incompatible alleles purge each other until there is only one left, usually at a lower frequency if not also under positive selection. Thus, classical DMI alleles are often at the state of neutral equilibrium that can be perturbed to arbitrary frequencies. However, epistatic selection can also lead to bistable systems [27, 28]. The time scale of collapse fundamentally changes if metastable equilibriums arise in epistatic selection. In a large population, metastable systems tend to be trapped in one stable equilibrium for a waiting time inversely proportional to the exponential of the noise at that equilibrium, before hopping to a different stable equilibrium [29]. In the regulatory DMI model, we have determined that the existence of a metastable frequency of haplotype AB in the focal population depends on the competition between hybridization that brings the foreign haplotype ab into the focal population, and recombination that breaks them up, thus exposing the DMI alleles to selection.

If AB's metastable haplotype frequency is highly robust to gene flow ($\gamma \gg 8$), we show in SI Appendix D that the mean collapse time is approximately

$$\langle T_d\rangle \approx \frac{\pi\left(\frac{2}{\gamma-2}\right)^{mN}\left(1+\frac{1}{\gamma}\right)e^{mN\left(\frac{\gamma}{4}-1\right)}}{\sqrt{\left(\frac{\gamma}{2}-1\right)\left(1-\frac{2\gamma}{(\gamma-2)^2}\right)}}, \tag{9}$$

which we call the Gaussian approximation, as it takes the metastable haplotype frequency distribution as a Gaussian.

For situations where the metastable frequency is less robust (γ is slighly larger than 8), we derived a beta-approximation of $\langle T_d\rangle$ given by:

$$\langle T_d\rangle \approx mN\mathrm{B}(K_1+1,K_2+1)\mathrm{B}(K_3+1,K_4+1) \times \frac{e^{mN\gamma\theta_{**}(1-\theta_{**})}}{e^{mN\gamma\theta_*(1-\theta_*)}}\frac{{\theta_*}^{-K_1-1}(1-\theta_*)^{-K_2+mN-1}}{{\theta_{**}}^{K_3}(1-\theta_{**})^{K_4+mN}} \tag{10}$$

where B is the beta function, and θ_*, θ_{**} are respectively the most and the least likely frequencies of haplotype AB given that the system currently stays metastable. Constants $K_1,\cdots,K_4$ specify the shape of the Beta distribution, and are given in Materials and Methods.

Both formulae scale as

$$\left(\frac{1}{\gamma}\right)^{mN+\frac{1}{2}}\exp\left(\frac{1}{4}mN\gamma\right)\approx\left(\frac{2r}{m}\right)^{mN+\frac{1}{2}}\exp\left(\frac{1}{2}Nr\right)$$

for sufficiently large γ. Neglecting the prefactor, the predominant time scale of collapse is exponentially dependent on $\frac{1}{2}Nr$, an analogue of the effective recombination rate in classical diffusion models [30]. Compared to classical DMIs, recombination affects the time scale of collapse in a completely opposite way. In the former system, especially with (co)dominant incompatible alleles, the ancestral haplotype has to be created by recombination in order to invade, but recombination in

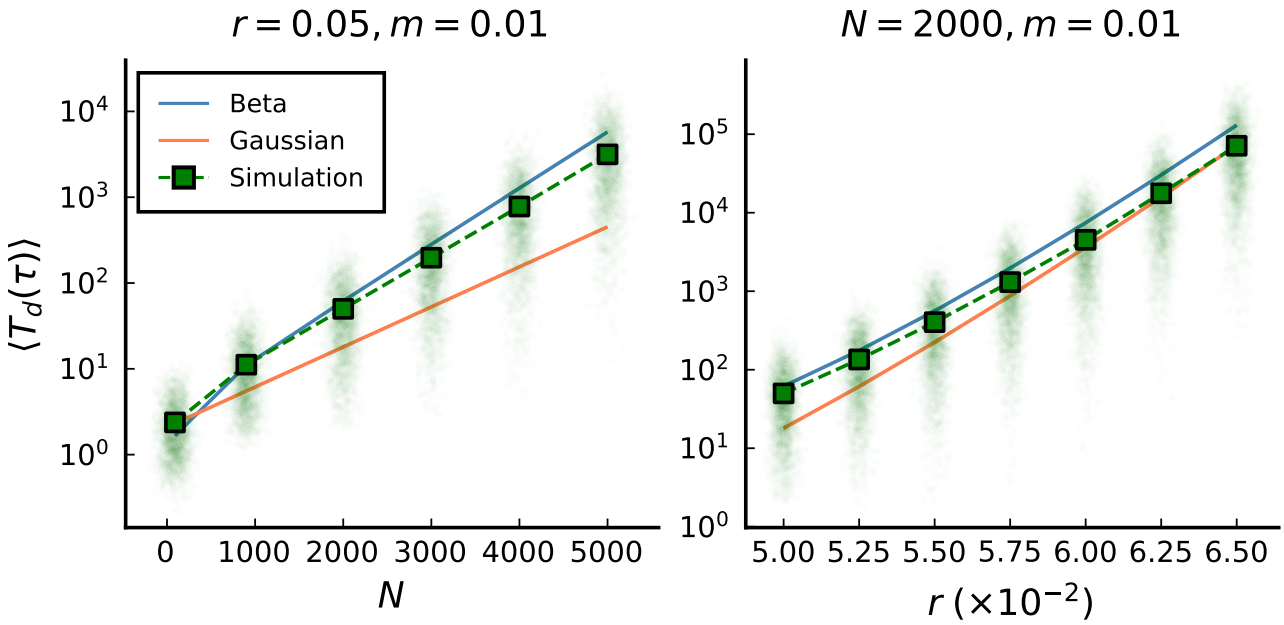

Figure 3: The mean collapse time under regulatory DMIs. The incompatibility is assumed to be symmetric and additive ($h_1' = h_3' = 1/2, h_2' = h_4' = 1, s = 10$). Equilibrium population size N and recombination probability r are allowed to vary. For each combination of parameters we simulated 3000 replicates of the entire birth-death process with fixed parameters $\alpha = 1, \mu = 0.1, m = 0.01$ and calculated the average T_d. The Beta approximation is more accurate than the Gaussian when N or r is small, but they both predict an exponential dependency of $\langle T_d \rangle$ on Nr.

the current system breaks apart co-adapted components in a regulatory pathway, thus blocking the invasion of the foreign haplotype.

Figure 3 shows the mean collapse time of the full birth-death model under regulatory DMIs and the two approximations. They clearly depict an exponential dependency of the average lifespan on both recombination probability and population size. When population size is large, the lifespan is extremely sensitive to minor changes in recombination probability.

The probability of restoring classical DMIs after gene flow ceases

Previously, we assumed that hybridization persisted indefinitely with the same probability in a demographically static population. Nevertheless, in a real population, hybridization may end if individuals move away from contact zones. Incompatibility can also drive the selection for modifiers that reduce inter-population mating ("reinforcement"). Without ongoing hybridization, a DMI may eventually recover in the focal population if some DMI alleles have remained. This is likely to happen with classical DMIs because their DMI alleles can be at neutral equilibriums and subsequently drift to fixation, while regulatory DMIs are unlikely to recover once its alleles dip below the critical frequency of its bistability.

Let us consider that the focal population with a classical DMI becomes isolated again at time τ, and let $Z(\tau)$ be the restoration probability. At the time of isolation, if the frequency of haplotype aB is θ_2 among the individuals, we can approximate the conditional probability of aB's fixation $P_{\text{fix}}(\theta_2)$ by θ_2 as haplotypes containing A is very rare, such that fixation is almost neutral. The distribution of θ_2 among the isolated individuals follows a sampling distribution $\mathcal{S}(\theta_2|\theta_2')$, where θ_2' represents the frequency of aB prior to isolation. Let $p(\theta_2', \tau)$ be the transition density of the frequency of aB in the focal population, then $Z(\tau) = \int_0^1 \mathrm{d}\theta_2 \int_0^1 P_{\text{fix}}(\theta_2)\mathcal{S}(\theta_2|\theta_2')p(\theta_2', \tau)\,\mathrm{d}\theta_2' = \int_0^1 \mathbb{E}_{\mathcal{S}}(\theta_2|\theta_2')p(\theta_2', \tau)\,\mathrm{d}\theta_2' \gtrsim \mathbb{E}_p(\theta_2'; \tau)$. We have assumed that the expectation of the sampling distribution

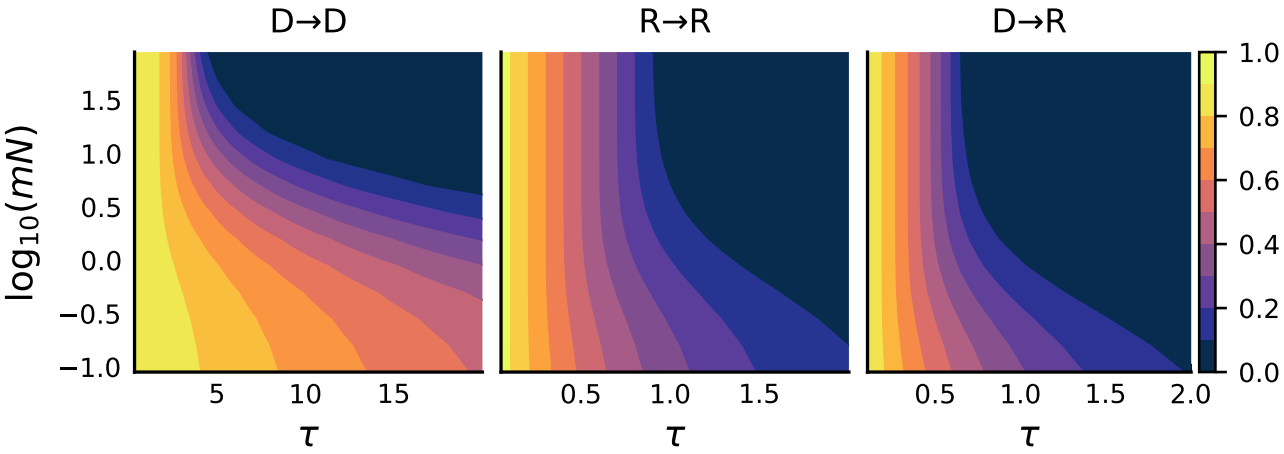

Figure 4: The lower bound of restoration probability $Z(\tau)$ for classical DMIs (D=dominant, R=recessive). Hybridization probability $m = 10^{-5}$ is held fixed. However, the population size increases and the magnitude of genetic drift decreases up the y-axis. The effect of genetic drift on $Z(\tau)$ is most prominent for dominant-dominant DMIs, and in all cases it increases the probability of restoration.

$\mathbb{E}_{\mathcal{S}}(\theta_2|\theta_2')$ is greater or equal to the original frequency θ_2' in the focal population. For example, if isolation is due to reinforcement related to incompatibilities, then aB will be over-represented in newly isolated individuals, thus $\mathbb{E}_{\mathcal{S}}(\theta_2|\theta_2') > \theta_2'$. Evaluating the integral using the forward-time solution of $p(\theta_2', \tau)$ gives the following series representation of the restoration probability (Figure 4):

$$\begin{aligned} &Z(\tau) \\ &\gtrsim \sum_{i=0}^{\infty} \frac{(-1)^i (2i + 2\tilde{u}_2 - \tilde{u}_1 + 1)\Gamma(i + 2\tilde{u}_2 - \tilde{u}_1 + 1)}{i! e^{\nu_i \tau} \Gamma(\tilde{u}_2)\Gamma(\tilde{u}_2 - \tilde{u}_1)(\tilde{u}_2 + i)_2 (\tilde{u}_2 - \tilde{u}_1 + i)_2} \\ &\approx \frac{u_2}{u_1} - \left(\frac{u_2}{u_1} - 1\right) \exp(-u_1 \tau), \quad \text{weak drift} \\ &\approx \exp[-(\tilde{u}_1 + 1)(u_2 - u_1)\tau], \quad \text{strong drift} \end{aligned} \tag{11}$$

Figure 4 depicts how the lower bound of classical DMI's $Z(\tau)$ varies with dominance, genetic drift and isolation time. In general, genetic drift increases the restoration probability, and the increment is mainly explained by the higher probability that haplotype aB will re-fix in the source population when genetic drift dominates.

C. DISCUSSION

Temporal patterns of post-zygotic reproductive barriers between incipient species

The correlation between species divergence and hybrid incompatibility is prevalent in nature. It has also been shown theoretically that the number of incompatibilities could "snowball" between isolated populations [5, 31]. Nonetheless, if gene flow persists long after speciation, collapse of DMIs is also a likely outcome. These contradictory predictions of the abundance of post-zygotic genetic barriers in natural populations are both partially supported by empirical evidence [32, 33, 34, 35]. Previous theories attribute the presence of DMIs in hybridizing populations to locally adaptive DMI alleles that resist purging, or they invoke multilocus epistasis [9, 36, 37]. Notably, these conclusions are mainly drawn at evolutionary equilibrium, while observed patterns of DMI in hybridizing populations is more likely under the influence of both accumulation and erosion of DMIs, and may be far from equilibrium if hybridization started only recently. Our results have focused entirely on the "erosion" part of the problem, which has been historically overlooked. We summarize each evolutionary force's effect on a DMI's lifespan as follows.

- Selection will directly influence the lifespan only when F_1 hybrids are incompatible. Without selection in F_1, the lifespan will almost entirely depend on the interplay among recombination, genetic drift, and gene flow. (The phenomenon that incompatibilities only appear after the second generation is known as hybrid-breakdown [38].)

- Recombination can either increase or decrease the lifespan depending on the underlying mechanisms of DMIs. Particularly, it decreases the lifespan of DMIs caused by mutually antagonistic alleles on different loci (classical), but it increases the lifespan of DMIs caused by disrupting co-evolved alleles (regulatory).

- With strong genetic drift, the average lifespan only depends on the initial rate of collapse as the detailed dynamics are masked by noise. If selection against F_1 is also strong, strong genetic drift will pose a barrier to DMI's collapse, a barrier produced by the frequent total extinction of F_1s before they contribute meaningful numbers of offsprings [39]. With weak genetic drift, regulatory DMIs have a better chance of staying stable in the long term, which corroborates the simulation by Lindtke et al [17].

Natural selection on DMI alleles

There has been recent evidence where the incompatible alleles are under some level of positive or balancing selection by themselves [40, 41, 42, 43], which has been ignored altogether in our model. Selection maintaining DMI alleles in their own population will in general prolong the lifespan, but disentangling this form of selection from selection against incompatibilities will be challenging in a hybrid zone, because both of them tend to restrict gene flow and distort local ancestries around DMI loci [44, 6].

On the other hand, neutrality (or quasi-neutrality) of the evolution of DMI alleles is a common and perhaps a realistic assumption, because such incompatibilities can readily evolve in a population under stabilizing selection. For instance, this mechanism is explicitly modeled as a neutral random walk on fitness hypercubes in the percolation theory of speciation [45], or as the quasi-neutral evolution of gene-regulatory networks [21, 14, 46, 15]. The neutrality assumption is also likely to be valid since most mutations are nearly neutral or deleterious [47]. A significant proportion of derived alleles currently observed in the population are thus likely to have been substituted neutrally, and some of these may cause multi-locus incompatibility with another population upon hybridization. We therefore conjecture that DMIs with no underlying selection for each individual allele could be a common form of incompatibility between pairs of populations that have recently come into secondary contact.

The relevance of the two-locus DMI model in nature

Existing theories of genetic incompatibilities can be grouped into two classes of models based on how epistasis is constructed. In the first class, usually limited to 2-4 loci, fitness has to be precisely defined for each genotype via additive/dominant/epistatic coefficients, thus quickly leading to a large number of parameters and variables. The best studied of this class is still the two-locus system [48]. Among the other class of models, usually a very large number of loci are considered, and fitnesses are either taken to be random [49], or are defined for some quantitative traits instead of the underlying genotypes, and then assume a trait-evolution model [50]. These models thus overcome the difficulty in multilocus analysis and are used in genome-scale theory of speciation and hybrid incompatibilities. While general theories with a large number of loci have indeed predicted several empirical patterns (e.g., Haldane's Rule), it is difficult to envision their applicability in a particular genetic system as genes are implicit in that framework. In reality, many deciphered DMIs involve a small set of loci with strong effects, such as the *Hmr-Lhr* system between *Drosophila melanogaster* and *D. simulans* [51]; the *hl13-hl14* incompatibility caused by gene duplication between monkeyflowers *Mimulus guttatus* and *M. nasutus* [52]; and the *MRS1-cox1* cytonuclear incompatibility between *Saccharomyces cerevisiae* and *S. paradoxus* [53]. If a particular pair of loci are strongly incompatible as compared to other incompatibilities be-

tween hybridizing populations, the influence of genomic background will be weak, and the two-locus model, or models with a small number of loci with strong effects, will be appropriate for that particular system. However, caution must be taken if standing variation in genomic background significantly alters incompatibilities [54], or if multiple DMIs influence each other via linked selection.

The ambivalent role of recombination in maintaining species' genetic boundaries

Commonly, suppressing recombination is thought to ramp up divergence between lineages because it will separate populations on different fitness peaks. A classic example is the prevalence of "speciation genes" in chromosomal inversions [55]. However, it relies on the assumption that species divergence is mainly the result of divergent selection on multiple loci. Under the process of developmental system drift, the entire molecular network of an individual is treated as a co-adapted unit in speciation. Each independently evolved population represents one possible realization of an optimal phenotype through subtle tuning in the underlying molecular network. Network dynamics are often disrupted in the recombined hybrids between different species (e.g., F_2 or backcrosses) [56, 15].

The role of recombination is reversed if incompatibilities are attributed to developmental system drift. If two populations initially fixed for different genotypes come into secondary contact, selection is only effective when there is enough recombination to expose the underlying genotypic differences in recombined individuals (assuming that F_1 is relatively fit). Without recombination, different genotypes will diffuse into each other almost neutrally, some of which can easily go extinct in a small population. In the regulatory DMI model, incompatibility on average collapses on a time scale proportional to $\exp(Nr/2)$. As *cis*-regulatory elements are often found in the vicinity of genes [57], Nr can be small even in a large population, and it is likely that this kind of DMI will not endure long-term hybridization, unless long-range *cis*-regulatory elements are involved [58]. Nonetheless, *trans*-regulatory elements are usually unlinked to their targets, and so there will be considerable recombination to guarantee a long lifespan of a DMI consisting *trans*-regulatory elements.

Quantifying the dynamics in natural populations

Hybridizing populations are not rare in nature, and some have been recently investigated for negative hybrid epistasis [13], but long-term time-series of evolution of the relevant genes are scarce [12], partially because sampling allele frequencies through time is costly and slow in many species. Thus, the extent to which DMIs collapse in natural populations is still largely unknown. However, there may exist a few indirect methods to detect collapse which we list below without providing rigorous proof.

If hybridizing populations are widely distributed with a narrow hybrid zone, we can compare the level of incompatibilities among individuals within and away from the hybrid zone. With bidirectional gene flow, classical DMI alleles will collapse on both side, and hybrid individuals will become more compatible closer to the hybrid zone. The dynamics with regulatory DMIs will be more intricate. Around the hybrid zone, if recombination is low, two haplotypes can diffuse into each other's parental population, and within-population incompatibility will soon equal between-population incompatibility near the hybrid zone; if recombination is high, two haplotypes can form a geographic cline analogous to an underdominant locus, whose center can diffuse away from the hybrid zone [27]. Different geographic patterns of DMI imply different underlying mechanisms and robustness to hybridization, which are worth further investigation [59].

If populations are panmictic, spatial methods no longer work, but we can look for genomic signatures of DMI collapse. Assuming bidirectional gene flow between parental populations, a collapsing classical DMI will likely resemble asymmetric introgression with opposite directions at the two loci, where derived alleles are replaced by ancestral ones. The exact signal may also resemble soft selective sweeps if hybridization is frequent [60], because ancestral haplotypes recovered by recombination can sweep to fixation. For regulatory DMIs, if recombination is low, two haplotypes will min-

gle up before selection drives one to extinction, thus the overall signal will perhaps also look like soft sweeps in both populations; If recombination is high, two haplotypes will be at migration-selection balance, and collapse will not be readily observable.

D. CONCLUSION

In Darwin's terms, evolution is often viewed as a creative process, the science of "the origin of species." However, reversal of speciation has often been overlooked. Recent studies show that gene flow has been important between many branches of the tree of life, especially between incipient species [61]. It creates ample opportunities for populations to interbreed post-speciation. In this paper, we show that the fusion of differentiated species into a compatible unit, in the sense of purging DMIs, can be as complex as speciation itself. Hybrid incompatibility is only one of many factors correlated with the speciation process, and the correlation will disappear if species interbreed, although the time scale of incompatibility loss can vary greatly. Consequently, defining species based only on current interspecific incompatibility does not guarantee their reliability. Further investigation of the collapse process will be necessary to better understand the evolution of hybrid incompatibilities during speciation.

E. MATERIALS AND METHODS

Details of the birth-death process

For 2 bi-allelic loci, there are 4 haplotypes and 10 phased two-locus diploid genotypes. Let $j = 0, \cdots, 9$ be the index of each genotype, and let n_j be the number of the j-th genotype. For each individual, a birth event happens with a fixed rate α, where the same individual mates with a random partner to produce exactly 1 offspring using a randomly selected haploid gamete from each parent. Due to ongoing hybridization, the partner is chosen randomly from the source population with probability m, and from its own population with probability $1-m$. The probability of recombination between loci is r. Independently of reproduction, each individual of the j-th genotype dies with rate $\mu + s_j + \beta \sum_j n_j$, where μ is the baseline death rate of all individuals, s_j is the genotype-specific death rate that drives viability selection, and β controls the population size. The full model can be described using a 1-step Markov jump process.

With the assumption of rare hybridization, stochastic differential equations [12] completely describe the evolution of haplotype frequencies θ_k in the focal population. Equation [12] formally recovers the classical diffusion approximation of the two-locus Wright-Fisher model [62, 63], but without measuring time in generations. Here, $S_k(\boldsymbol{\theta})$ is the selection function on haplotype k; $\theta_k^* - \theta_k$ describes the change of haplotype frequencies due to hybridization, where θ_k^* is the constant frequency of haplotype k in the source population; $D(\boldsymbol{\theta})$ is the usual measure of linkage disequilibrium [64], and the sign depends inversely on whether the haplotype contributes to positive or negative linkage disequilibrium. $\xi_{\theta_k}(\tau)$ are inter-correlated white noises driving genetic drift. The full derivation and the covariance of the noise terms are shown in SI Appendix A. Readers should also refer to SI Appendix B for deriving the 1-D approximations of haplotype frequencies from [12].

$$\partial_\tau \theta_k = S_k(\boldsymbol{\theta}) + (\theta_k^* - \theta_k) \pm \gamma D(\boldsymbol{\theta}) + \xi_{\theta_k}(\tau)/\sqrt{\lambda} \tag{12}$$

Simulating the birth-death process

The full birth-death process was simulated in `Julia v1.5` using the Gillespie algorithm implemented in the package `DifferentialEquations.jl`. For a large population, the process is approximated by the tau-leaping algorithm [65], where during a fixed small time interval $[t, t+\Delta t]$, the numbers of jumps of each type are drawn from Poisson distributions using the rates at time t, and the process leaps forward to $t + \Delta t$ by updating the variables using the numbers of jumps. The code is available at https://github.com/tzxiong/2020_The_collapse_of_genetic_incompatibilities. Symbolic computation was performed in `Mathematica v12.1` [66].

Calculating the distribution of T_d for classical DMIs

A general one dimensional Ito stochastic differential equation $\partial_\tau \theta(\tau) = u(\theta) + \sigma(\tau)\,\mathrm{d}W_\tau$ on $[0,1]$ corresponds uniquely to a Fokker-Planck equation $\partial_\tau p(\theta,\tau) = -\partial_\theta J(\theta,\tau)$, where $p(\theta,\tau)$ is the transition density, and

$$J(\theta,\tau) = u(\theta)p(\theta,\tau) - \frac{1}{2}\partial_\theta \sigma^2(\theta)p(\theta,\tau) \tag{13}$$

stands for the probability current. If the boundary at 1 is reflecting, the distribution of the first hitting time (the collapse time) at 0 is

$$f_{T_d}(\tau) = -\partial_\tau \int_0^1 p(\theta,\tau)\,\mathrm{d}\theta = -J(0,\tau) \tag{14}$$

The beta-approximation of $\langle T_d \rangle$ for regulatory DMIs

Provided that haplotype frequency θ_0 is still trapped at the metastable equilibrium, we can approximate the conditional equilibrium distribution of θ_0 as a beta function with the same peak and the same curvature around the peak (SI Appendix D). It leads to the form of $\langle T_d \rangle$ expressed in [10], where θ_* is given by the largest solution of equation $-mN\gamma(1-2\theta) - \frac{1}{\theta} - \frac{mN-1}{1-\theta} = 0$ in terms of θ, and θ_{**} is given by $\frac{3}{4} - \frac{1}{4}\sqrt{1-8/\gamma}$. Constants $K_1, \cdots, K_4$ are given by

$$\begin{aligned}
K_1 &= \frac{mN{\theta_*}^2[1-2\gamma(1-\theta_*)^2]}{1-\theta_*} + 2\theta_* - \frac{1}{1-\theta_*} \\
K_2 &= mN\theta_*[1-2\gamma(1-\theta_*)^2] - 2\theta_* - \frac{1}{\theta_*} + 2 \\
K_3 &= \frac{mN\theta_{**}[1-2\gamma(1-\theta_{**})^2]}{2\theta_{**}(1-\theta_{**})-1}\theta_{**} \\
K_4 &= \frac{mN\theta_{**}[1-2\gamma(1-\theta_{**})^2]}{2\theta_{**}(1-\theta_{**})-1}(1-\theta_{**})
\end{aligned} \tag{15}$$

References

[1] Maheshwari, S & Barbash, D. A. (2011) The genetics of hybrid incompatibilities. *Annual review of genetics* **45**, 331–355.

[2] Dobzhansky, T. (1937) *Genetics and the origin of species.* (New York: Columbia University Press).

[3] Muller, H. (1942) *Isolating mechanisms, evolution, and temperature.* Vol. 6, pp. 71–125.

[4] Orr, H. A. (1995) The population genetics of speciation: the evolution of hybrid incompatibilities. *Genetics* **139**, 1805–1813.

[5] Orr, H. A & Turelli, M. (2001) The evolution of postzygotic isolation: accumulating dobzhansky-muller incompatibilities. *Evolution* **55**, 1085–1094.

[6] Smith, J, Payseur, B, & Novembre, J. (2018) Expected patterns of local ancestry in a hybrid zone. *bioRxiv.*

[7] Kirkpatrick, M. (2001) Reinforcement during ecological speciation. *Proceedings of the Royal Society of London. Series B: Biological Sciences* **268**, 1259–1263.

[8] Barton, N & Bengtsson, B. O. (1986) The barrier to genetic exchange between hybridising populations. *Heredity* **57**, 357–376.

[9] Bank, C, Bürger, R, & Hermisson, J. (2012) The limits to parapatric speciation: Dobzhansky–muller incompatibilities in a continent–island model. *Genetics* **191**, 845–863.

[10] Blanckaert, A, Bank, C, & Hermisson, J. (2020) The limits to parapatric speciation 3: Evolution of strong reproductive isolation in presence of gene flow despite limited ecological differentiation. *bioRxiv.*

[11] Rosser, N, Queste, L. M, Cama, B, Edelman, N. B, Mann, F, Mori Pezo, R, Morris, J, Segami, C, Velado, P, Schulz, S, et al. (2019) Geographic contrasts between pre-and postzygotic barriers are consistent with reinforcement in heliconius butterflies. *Evolution* **73**, 1821–1838.

[12] Zuellig, M. P & Sweigart, A. L. (2018) A two-locus hybrid incompatibility is widespread, polymorphic, and active in natural populations of mimulus. *Evolution* **72**, 2394–2405.

[13] Powell, D. L, García-Olazábal, M, Keegan, M, Reilly, P, Du, K, Díaz-Loyo, A. P, Banerjee, S, Blakkan, D, Reich, D, Andolfatto, P, et al. (2020)

Natural hybridization reveals incompatible alleles that cause melanoma in swordtail fish. *Science* **368**, 731–736.

[14] True, J. R & Haag, E. S. (2001) Developmental system drift and flexibility in evolutionary trajectories. *Evolution & development* **3**, 109–119.

[15] Schiffman, J. S & Ralph, P. L. (2017) System drift and speciation. *BioRxiv* p. 231209.

[16] Porter, A. H & Johnson, N. A. (2002) Speciation despite gene flow when developmental pathways evolve. *Evolution* **56**, 2103–2111.

[17] Lindtke, D & Buerkle, C. A. (2015) The genetic architecture of hybrid incompatibilities and their effect on barriers to introgression in secondary contact. *Evolution* **69**, 1987–2004.

[18] Wright, S. (1931) Evolution in mendelian populations. *Genetics* **16**, 97.

[19] Gavrilets, S. (1997) Evolution and speciation on holey adaptive landscapes. *Trends in ecology & evolution* **12**, 307–312.

[20] Khatri, B. S & Goldstein, R. A. (2019) Biophysics and population size constrains speciation in an evolutionary model of developmental system drift. *PLoS computational biology* **15**, e1007177.

[21] Johnson, N. A & Porter, A. H. (2000) Rapid speciation via parallel, directional selection on regulatory genetic pathways. *Journal of Theoretical Biology* **205**, 527–542.

[22] Barton, N. H & De Cara, M. A. R. (2009) The evolution of strong reproductive isolation. *Evolution: International Journal of Organic Evolution* **63**, 1171–1190.

[23] Takahasi, K. R, Matsuo, T, & Takano-Shimizu-Kouno, T. (2011) Two types of cis-trans compensation in the evolution of transcriptional regulation. *Proceedings of the National Academy of Sciences* **108**, 15276–15281.

[24] Mack, K. L, Campbell, P, & Nachman, M. W. (2016) Gene regulation and speciation in house mice. *Genome research* **26**, 451–461.

[25] Karlin, S & Taylor, H. E. (1981) *A second course in stochastic processes.* (Elsevier).

[26] Iyer-Biswas, S & Zilman, A. (2016) First-passage processes in cellular biology. *Advances in Chemical Physics* **160**, 261–306.

[27] Barton, N. H. (1979) The dynamics of hybrid zones. *Heredity* **43**, 341–359.

[28] Barton, N. H & Turelli, M. (2011) Spatial waves of advance with bistable dynamics: cytoplasmic and genetic analogues of allee effects. *The American Naturalist* **178**, E48–E75.

[29] Kramers, H. A. (1940) Brownian motion in a field of force and the diffusion model of chemical reactions. *Physica* **7**, 284–304.

[30] Ohta, T & Kimura, M. (1969) Linkage disequilibrium due to random genetic drift. *Genetics Research* **13**, 47–55.

[31] Kondrashov, A. S. (2003) Accumulation of dobzhansky-muller incompatibilities within a spatially structured population. *Evolution* **57**, 151–153.

[32] Schumer, M & Brandvain, Y. (2016) Determining epistatic selection in admixed populations. *Molecular Ecology* **25**, 2577–2591.

[33] Ostevik, K. L, Rifkin, J. L, Xia, H, & Rausher, M. D. (2020) Morning glory species co-occurrence is associated with asymmetrically decreased and cascading reproductive isolation. *Evolution Letters.*

[34] Barth, J. M, Gubili, C, Matschiner, M, Tørresen, O. K, Watanabe, S, Egger, B, Han, Y.-S, Feunteun, E, Sommaruga, R, Jehle, R, et al. (2020) Stable species boundaries despite ten million years of hybridization in tropical eels. *Nature communications* **11**, 1–13.

[35] Simon, A, Fraïsse, C, El Ayari, T, Liautard-Haag, C, Strelkov, P, Welch, J. J, & Bierne, N. (2020) How do species barriers decay? concordance and local introgression in mosaic hybrid zones of mussels. *Journal of Evolutionary Biology* **00**, 1–16.

[36] Paixão, T, Bassler, K. E, & Azevedo, R. B. R. (2015) Emergent speciation by multiple dobzhansky–muller incompatibilities. *bioRxiv*.

[37] Coughlan, J. M & Matute, D. R. (2020) The importance of intrinsic postzygotic barriers throughout the speciation process. *Philosophical Transactions of the Royal Society B* **375**, 20190533.

[38] Oka, A, Mita, A, Sakurai-Yamatani, N, Yamamoto, H, Takagi, N, Takano-Shimizu, T, Toshimori, K, Moriwaki, K, & Shiroishi, T. (2004) Hybrid breakdown caused by substitution of the x chromosome between two mouse subspecies. *Genetics* **166**, 913–924.

[39] Kimura, M. (1980) Average time until fixation of a mutant allele in a finite population under continued mutation pressure: Studies by analytical, numerical, and pseudo-sampling methods. *Proceedings of the National Academy of Sciences* **77**, 522–526.

[40] Seidel, H. S, Rockman, M. V, & Kruglyak, L. (2008) Widespread genetic incompatibility in c. elegans maintained by balancing selection. *science* **319**, 589–594.

[41] Maheshwari, S, Wang, J, & Barbash, D. A. (2008) Recurrent positive selection of the drosophila hybrid incompatibility gene hmr. *Molecular biology and evolution* **25**, 2421–2430.

[42] Todesco, M, Balasubramanian, S, Hu, T. T, Traw, M. B, Horton, M, Epple, P, Kuhns, C, Sureshkumar, S, Schwartz, C, Lanz, C, et al. (2010) Natural allelic variation underlying a major fitness trade-off in arabidopsis thaliana. *Nature* **465**, 632–636.

[43] Case, A. L, Finseth, F. R, Barr, C. M, & Fishman, L. (2016) Selfish evolution of cytonuclear hybrid incompatibility in mimulus. *Proceedings of the Royal Society B: Biological Sciences* **283**, 20161493.

[44] Sedghifar, A, Brandvain, Y, & Ralph, P. (2016) Beyond clines: lineages and haplotype blocks in hybrid zones. *Molecular ecology* **25**, 2559–2576.

[45] Gavrilets, S & Gravner, J. (1997) Percolation on the fitness hypercube and the evolution of reproductive isolation. *Journal of theoretical biology* **184**, 51–64.

[46] Palmer, M. E & Feldman, M. W. (2009) Dynamics of hybrid incompatibility in gene networks in a constant environment. *Evolution: International Journal of Organic Evolution* **63**, 418–431.

[47] Eyre-Walker, A & Keightley, P. D. (2007) The distribution of fitness effects of new mutations. *Nature Reviews Genetics* **8**, 610–618.

[48] Karlin, S. (1975) General two-locus selection models: some objectives, results and interpretations. *Theoretical Population Biology* **7**, 364–398.

[49] Neher, R. A & Shraiman, B. I. (2009) Competition between recombination and epistasis can cause a transition from allele to genotype selection. *Proceedings of the National Academy of Sciences* **106**, 6866–6871.

[50] Simon, A, Bierne, N, & Welch, J. J. (2018) Coadapted genomes and selection on hybrids: Fisher's geometric model explains a variety of empirical patterns. *Evolution Letters* **2**, 472–498.

[51] Barbash, D. A, Roote, J, & Ashburner, M. (2000) The drosophila melanogaster hybrid male rescue gene causes inviability in male and female species hybrids. *Genetics* **154**, 1747–1771.

[52] Zuellig, M. P & Sweigart, A. L. (2018) Gene duplicates cause hybrid lethality between sympatric species of mimulus. *PLoS genetics* **14**, e1007130.

[53] Chou, J.-Y, Hung, Y.-S, Lin, K.-H, Lee, H.-Y, & Leu, J.-Y. (2010) Multiple molecular mechanisms cause reproductive isolation between three yeast species. *PLoS Biol* **8**, e1000432.

[54] Matute, D. R, Gavin-Smyth, J, & Liu, G. (2014) Variable post-zygotic isolation in d rosophila melanogaster/d. simulans hybrids. *Journal of evolutionary biology* **27**, 1691–1705.

[55] Butlin, R. K. (2005) Recombination and speciation. *Molecular Ecology* **14**, 2621–2635.

[56] Burton, R. S, Pereira, R. J, & Barreto, F. S. (2013) Cytonuclear genomic interactions and hybrid breakdown. *Annual Review of Ecology, Evolution, and Systematics* **44**, 281–302.

[57] Wittkopp, P. J & Kalay, G. (2012) Cis-regulatory elements: molecular mechanisms and evolutionary processes underlying divergence. *Nature Reviews Genetics* **13**, 59–69.

[58] Noonan, J. P & McCallion, A. S. (2010) Genomics of long-range regulatory elements. *Annual review of genomics and human genetics* **11**, 1–23.

[59] Gavrilets, S. (1997) Hybrid zones with dobzhansky-type epistatic selection. *Evolution* **51**, 1027–1035.

[60] Hermisson, J & Pennings, P. S. (2005) Soft sweeps: molecular population genetics of adaptation from standing genetic variation. *Genetics* **169**, 2335–2352.

[61] Arnold, M. L. (2015) *Divergence with genetic exchange.* (Oxford University Press).

[62] Ethier, S. N & Nagylaki, T. (1980) Diffusion approximations of markov chains with two time scales and applications to population genetics. *Advances in Applied Probability* **12**, 14–49.

[63] Ethier, S. N & Nagylaki, T. (1989) Diffusion approximations of the two-locus wright-fisher model. *Journal of mathematical biology* **27**, 17–28.

[64] Lewontin, R. C & Kojima, K. (1960) The evolutionary dynamics of complex polymorphisms. *Evolution* **14**, 458–472.

[65] Gillespie, D. T. (2001) Approximate accelerated stochastic simulation of chemically reacting systems. *The Journal of chemical physics* **115**, 1716–1733.

[66] Wolfram Research Inc. (2020) Mathematica, Version 12.1. Champaign, IL, USA.